

Deformation and Fracture Behavior of PP/Ash Composites

S. G. Pardo^a, C. Bernal^{b,*}, M. J. Abad^a, J. Cano^a and L. Barral Losada^a

^a Grupo de Polímeros, Departamento de Física, E.U.P.-Ferrol, Universidad de A Coruña, Avda. 19 febrero, s/n. 15405-Ferrol, España

^b Grupo de Materiales Avanzados, INTECIN (UBA-CONICET), Departamento de Ingeniería Mecánica, Facultad de Ingeniería, Universidad de Buenos Aires, Av. Paseo Colón 850, C1063ACV, Buenos Aires, Argentina

Received 3 September 2007; accepted 1 August 2008

Abstract

In the present work, the deformation and fracture behavior of PP/ash composites with different ash content was investigated. The effect of a silane coupling agent was also analyzed. From uniaxial tensile tests, an increase in the stiffness with ash content was found as a result of the incorporation of the stiffer filler within the PP matrix. On the other hand, a decrease in tensile strength and strain at break with filler loading was observed. This result was attributed to the increased number of debonded large particles with filler content, which subsequently led to the formation of critical-size flaws. On the other side, the composites displayed higher values of fracture parameters than the matrix as a result of the development of a particle induced toughening mechanism. However, fracture properties were also found to decrease with ash content. This could be attributed to the increase in the number of critical-size flaws that induced premature failure. The incorporation of a silane coupling agent in the formulations led to composites with slightly improved tensile and fracture properties. This was probably due to improved interaction between PP and ash in the first case and a better dispersion of ash particles in the matrix and/or changes in the crystallization behavior of PP, in the latter case.

© Koninklijke Brill NV, Leiden, 2009

Keywords

Polymer composites, polypropylene, rigid fillers, deformation behavior, fracture behavior, silane treatment

1. Introduction

The incorporation of inorganic fillers in polymers is a widely used practice in industry to obtain new plastics with better properties at relatively low cost.

Furthermore, the increasing interest of current industries to re-use their wastes is mainly driven by economic and ecological reasons. Ashes are an appealing alternative for mineral fillers, which also fill the environmental requirement. They are cheaper and more environmentally friendly. They are solid industrial wastes pro-

* To whom correspondence should be addressed. E-mail: cbernal@fi.uba.ar

duced as the result of the combustion of carbon and other fossil fuels. Inorganic ashes are generally mainly composed of a significant amount of SiO_2 and lower contents of Al_2O_3 , Fe_2O_3 , Na_2O , MgO , K_2O , etc.

The use of ash as reinforcement in polymer composites has been already reported in the literature [1–14].

Poor interfacial adhesion between inorganic fillers and polymers is frequently observed. Hence, different additives such as coupling agents able to react with the filler are often added in the formulations. They have reactive groups compatible with the chemical nature of the polymer and the filler [15, 16].

One of the most commonly used groups of coupling agents are the silanes [4] with two kinds of reactive groups (inorganic and organic) in a single molecule [17]. A chemical reaction between the filler functional groups (such as OH) and the alkoxy groups of silane is expected to occur during the treatment of the filler, creating a silane-functionalized surface. A protective layer able to prevent the agglomeration of the filler particles is also created by silane treatment.

On the other side, in many applications of polymers, mechanical properties are very important and, particularly, the optimization of the material toughness is often required. For this purpose, knowledge of the relationship between morphology and deformation behavior is needed.

In this work, the deformation and fracture behavior of PP/ash composites with raw ash and with ash treated with silane was investigated. The effect of the ash content was also studied.

2. Experimental

2.1. Materials

The fly ashes employed were obtained from biomass combustion (kindly supplied by Industrias del Tablero S.A. (INTASA)). The ashes were separated using a sieve of mesh 400 μm . Particle size distributions were determined from SEM micrographs of ash particles using imaging software.

The thermoplastic matrix was an isotactic polypropylene (PP 070G2M) delivered by Repsol-YPF, with a melt flow index of 12 g/10 min (230°C, 2.16 kg) and a density of 0.902 g/cm³. A commercially available polymer processing additive (Dynamar FX 5911, Dyneon, 3M Company) was used. The blend of PP and Dynamar will be referred to in this work as the PP matrix and the PP as neat PP.

A coupling agent (GF96 supplied by Wacker-Chemie Italia S.r.L.) 0.1 wt% with respect to the weight of ash was incorporated into the filler. The coupling agent was prepared in an aqueous solution at the concentration required. Then, treated ashes were dried in an oven at 105°C for 24 h.

2.2. Sample Preparation and Mechanical Characterization

Different contents of ash (10, 20 and 30 wt%) and polypropylene were mixed in a corotating twin-screw extruder (Brabender DSE20) at 200°C and 30 rpm.

Pellets of PP and the composites were compression-molded into 3 and 8 mm plaques at 220°C, under a pressure of 10 bar for 10 min followed by 50 bar for 20 min. Then, the plaques were rapidly cooled down by circulating water within the press plates under a pressure of 50 bar for 25 min. Thermal stresses generated during molding were released by annealing the plaques in an oven for 3 h at 100°C.

Uniaxial tensile tests were performed on dog-bone specimens in an Instron dynamometer 5566 at 5 mm/min in accordance with ASTM D-638-02 standard recommendations [18]. Stress–strain curves were obtained from these tests. Young's modulus, tensile strength and ultimate strain were determined from these curves. A minimum of six specimens were tested for each system, the average values of the mechanical parameters and their standard deviations were calculated.

Fracture characterization was carried out on single-edge notched bend SENB specimens cut out from compression-molded thick plaques (thickness, $B = 8$ mm).

Sharp notches were introduced by sliding a fresh razor blade into a machined slot. Crack-to-depth (a/W), thickness-to-depth (B/W) and span-to-depth (S/W) ratios were always kept equal to 0.5, 0.5 and 4, respectively.

Three-point-bend tests were performed in an Instron dynamometer 4467 at 1 mm/min.

Critical stress intensity factor (K_{IQ}) and energy release rate (G_{IQ}) values at initiation were obtained by following ASTM D-5045-92 standard recommendations [19].

Critical energy release rate values at propagation (G_{CP}) were also determined. They were calculated from the total area under the load–displacement curve (U_p), as follows [20]:

$$G_{CP} = U_p/B(W - a). \quad (1)$$

Unlike G_{IC} , that only takes into account the critical load for the onset of crack growth, G_{CP} mainly involves the crack propagation step.

2.3. Study of the Deformation Mechanism

To study the dominant deformation mechanism, some SENB specimens were also tested in three-point bending in the Instron dynamometer 4467, at the same speed used in the fracture tests (1 mm/min).

The specimens were tested up to subcritical displacement levels until some deformation was evident. Side surfaces had been previously polished with different abrasive papers of increasing coarseness. Then, they were observed by scanning electron microscopy (SEM) after they had been coated with a thin layer of gold.

All tests were carried out at room temperature.

2.4. Fracture Surface Analysis

The fracture surfaces of SENB specimens tested in fracture tests were examined using a JEOL JSM-6460LV scanning electron microscope (SEM) at an accelerating voltage of 20 kV. The samples were sputter coated with a thin layer of gold before they were observed.

Energy-dispersive X-ray analysis was also performed in a JEOL JSM 6400 scanning electron microscope (SEM) at an accelerating voltage of 20 kV to study the effect of the silane treatment on the interface.

3. Results and Discussion

3.1. Particle Size Distribution

The ash particles used were cenospheres, which consist of hollow particles containing a central porosity as well as porosity in the walls [21]. The crystalline phase of fly ash was composed by 2.7 vol% of quartz (SiO_2) and 17.0 vol% of kyanite (Al_2SiO_5) [22].

In addition, as normal ash was used, it was not well separated and uneven particle sizes, many coarse particles and irregularly shaped impurities were observed in all samples [5]. However, the diameter was assumed to be the characteristic geometric dimension.

Figure 1 presents the particle size distribution for ash particles. As can be observed in this figure, a monomodal size distribution exists with a mean diameter value of $30.88 \pm 16.42 \mu\text{m}$. Furthermore, a few particles having diameter higher than $100 \mu\text{m}$ can also be found.

3.2. Deformation Behavior

Figure 2 shows typical engineering stress–strain curves obtained in uniaxial tensile tests for the matrix and the composites with raw ash, as an example. It is observed

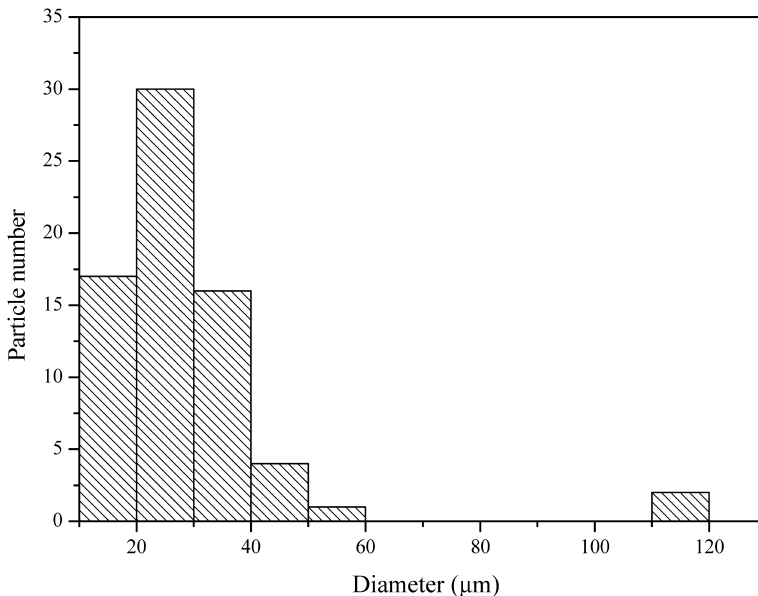


Figure 1. Particle size distribution of ash.

in this figure that the matrix and PP/ash samples displayed some degree of non-linearity before maximum stress. Complete failure of specimens occurred almost immediately after maximum stress was attained, with no necking before fracture.

Fracture surfaces of broken specimens exhibited stress whitening.

In addition, all composites displayed less ductility than PP matrix as a result of the poor interfacial adhesion between both ash and PP and the subsequent large particle debonding which induced premature failure.

Figure 3(a), 3(b) and 3(c) presents the values of Young's modulus, tensile strength and strain at break as a function of ash content, respectively along with their deviations.

An increasing trend of Young's modulus with filler content was observed in accordance with expectations. The incorporation of a much stiffer second phase in the matrix led to composites with improved stiffness [17].

On the other hand, tensile strength and strain at break values were found to decrease as the ash content increased, probably due to the debonding of large ash particles from the PP matrix. It has been established in the literature [23], that poor tensile strength and low failure strain might be caused by particle debonding from the matrix prior to yielding as a result of poor interfacial adhesion.

The incorporation of the silane coupling agent led to composites with slightly better properties, probably as a result of an improvement in the ash particle disper-

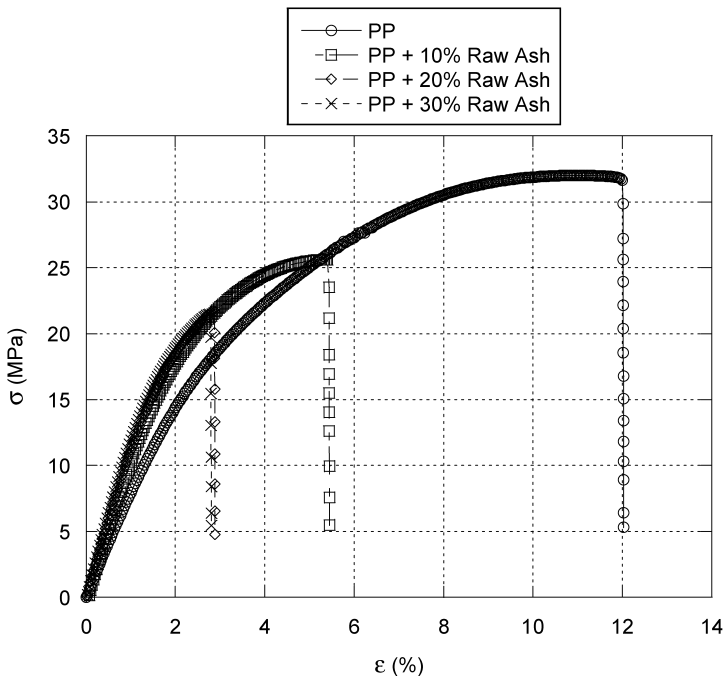


Figure 2. Engineering stress–strain curves for the PP matrix and the composites with raw ash as an example.

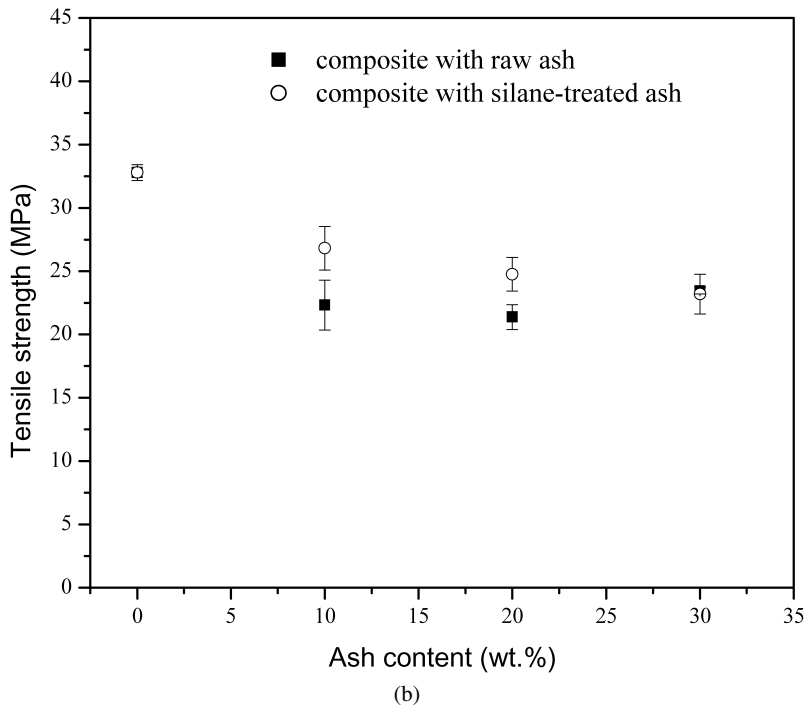
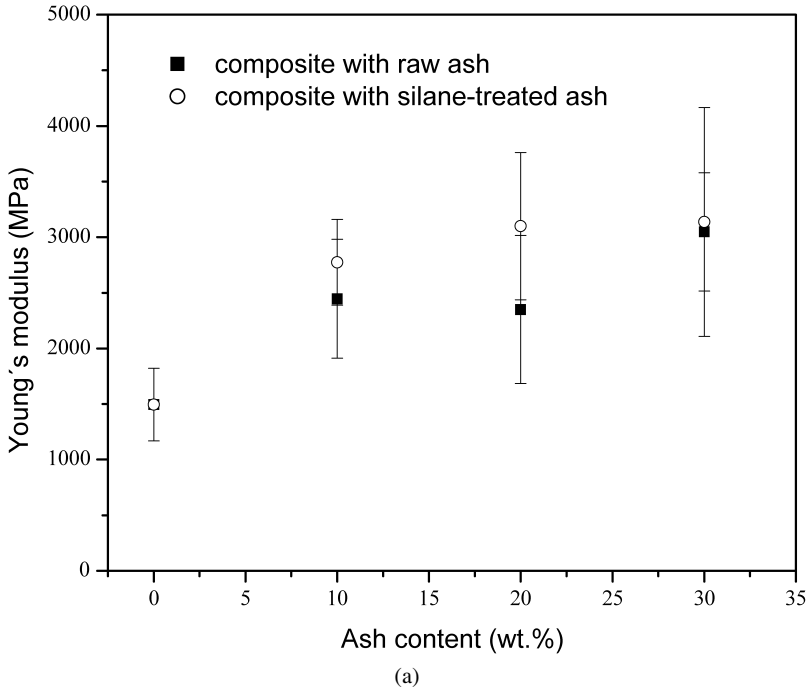


Figure 3. Tensile properties as a function of ash content for the different composites investigated: (a) Young's modulus; (b) tensile strength; (c) strain at break.

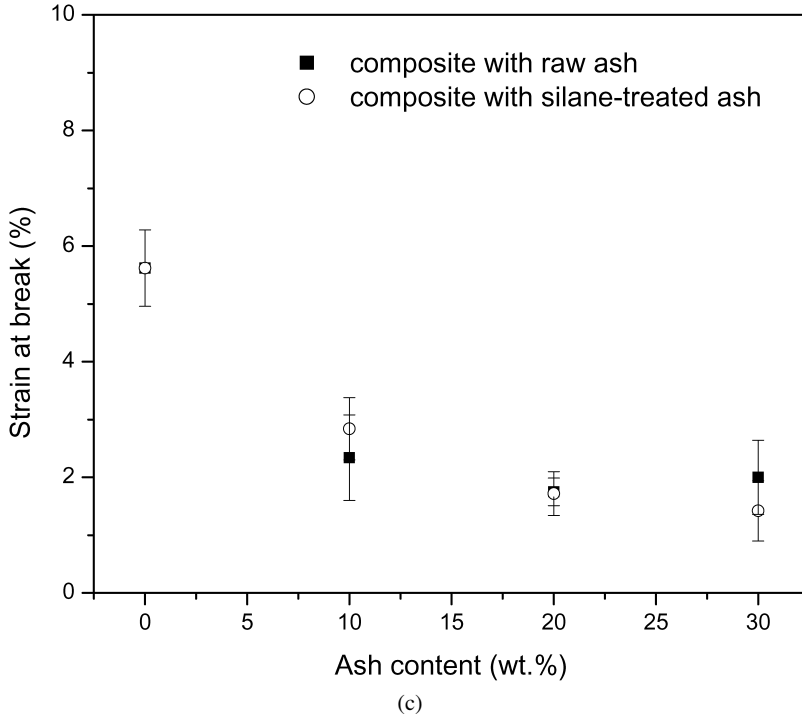


Figure 3. (Continued.)

sion and/or a better interaction between PP and ash. Similar results have been found in a recent work for PP–ash composites with 60 wt% ash [17].

3.3. Fracture Behavior

Some neat polypropylene samples exhibited non-linear load–displacement behavior with some amount of slow crack growth preceding unstable fracture, in agreement with the results reported in literature for polypropylene homopolymer [24, 25]. At the initial steps, stable crack propagation was observed and, at a certain point in the load–displacement curve, the propagation mode suddenly changed. Crack propagation became unstable and samples separated into two halves [25]. Other samples exhibited completely ductile fracture with nonlinear behavior until maximum load and a gradual decrease of load until zero. Slow crack growth preceded complete fracture.

The PP matrix and the composites displayed ductile fracture. In addition, fracture surfaces of broken specimens were stress whitened.

Figure 4 shows load–displacement curves for the PP matrix and the composites with raw ash, as an example.

Figure 5 shows a typical fracture surface for a composite specimen loaded to a subcritical displacement level and then unloaded. Complete fracture of the specimen was attained at high velocity in a Charpy pendulum after it had been immersed

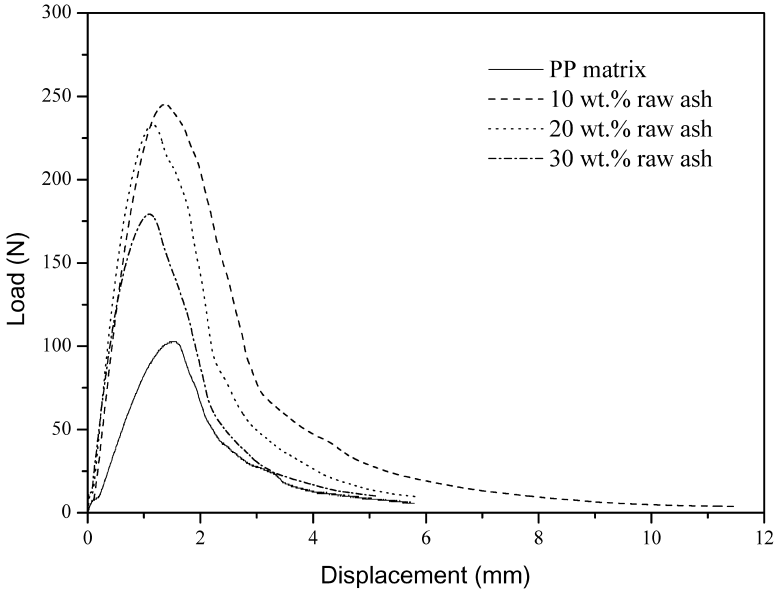


Figure 4. Load–displacement curves for the matrix and the composites with different content of raw ash as an example.

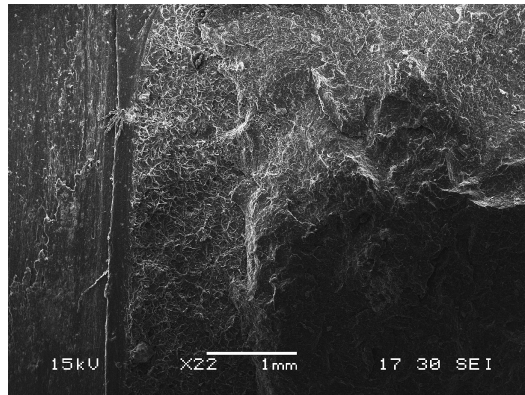


Figure 5. SEM micrograph of a typical fracture surface of a composite SENB specimen tested in three-point bending up to a subcritical displacement level. (The crack propagated from the left to the right.)

in liquid nitrogen for a few minutes. Matrix ductile tearing could be distinguished from the unstable fracture, which was promoted by the high velocity and low temperature in the Charpy pendulum. Otherwise, ductile tearing (slow crack growth) would have been extended through the whole ligament as was observed in the fracture samples that were tested until complete fracture.

According to linear elastic fracture mechanics [26], for valid plane strain fracture toughness determinations, linear-elastic behavior up to the point of fracture and plane strain conditions are simultaneously required. Although these requirements

Table 1.

Fracture parameters

wt% ash	K_{IQ} (MPa m ^{1/2})		G_{IQ} (kJ/m ²)		G_{CP} (kJ/m ²)	
	Raw ash	Treated ash	Raw ash	Treated ash	Raw ash	Treated ash
PP	1.94 ± 0.36	–	4.47 ± 0.74	–	5.25 ± 0.60	–
0	1.37 ± 0.13	–	3.66 ± 0.40	–	4.35 ± 0.63	–
10	2.93 ± 0.11	3.13 ± 0.14	7.09 ± 0.29	7.98 ± 0.67	10.19 ± 0.60	11.95 ± 0.87
20	2.84 ± 0.11	3.02 ± 0.43	5.96 ± 0.12	6.26 ± 0.27	8.20 ± 0.30	9.30 ± 0.62
30	2.70 ± 0.09	2.72 ± 0.06	5.22 ± 0.19	6.03 ± 0.20	7.26 ± 0.48	8.65 ± 0.26

were not satisfied in our experiments, the initiation parameter values still reflect a critical state for crack initiation [27]. Therefore, they were used here to compare the fracture initiation behavior of the materials.

The values of the fracture initiation parameters (K_{IQ} and G_{IQ}) are listed in Table 1. It is observed in this table that the incorporation of the processing additive to PP led to lower values of K_{IQ} and G_{IQ} whereas the material behavior was more ductile.

Irrespective of the presence of the coupling agent, a decreasing trend of the fracture initiation parameters with increasing ash content was observed (Table 1) probably due to the increase in the number of critical-size flaws that induced premature failure. However, all composites displayed higher critical initiation values than neat PP or the matrix as a result of the toughening induced by the presence of small ash particles, as will be shown later.

In addition, a significant improvement in the crack propagation resistance was found for the composites in comparison to the matrix (Table 1), as more energy was absorbed by the composite specimens to fracture (represented by the area under the load–displacement curve in Fig. 4). Poor adhesion between PP and ash was responsible for debonding at the PP/ash interface and hence, for inducing matrix stretching around small particles as it will be confirmed below. This mechanism required a large amount of energy [28, 29].

Furthermore, composite samples with treated ash displayed slightly higher values of fracture parameters, suggesting a positive effect of the incorporation of silane to ash.

3.4. Deformation Mechanism

A typical SEM micrograph of a lateral view of a composite SENB sample tested until some damage was developed, is shown in Fig. 6. It can be seen in this figure very small ash particles (particle size smaller than 1 μm) debonded from the matrix, which also elongated around them. The difference in the elastic properties between PP and ash made small ash particles act as stress concentrators during deformation processes and the triaxial stress around them to build up. Interfacial debonding occurred, changing the stress state in the surrounding matrix. The sensitivity of the

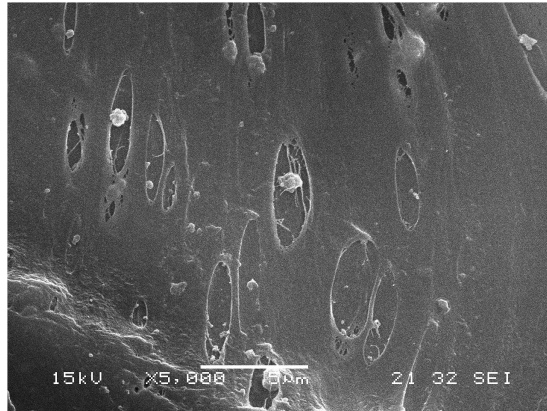


Figure 6. Typical side view of a composite SENB sample tested up to a subcritical displacement level under similar geometric conditions of those used in fracture tests.

matrix polymer toward crazing was reduced by the volume strain release and shear yielding was favored. This mechanism of toughening has been proposed by Kim and Michler [30, 31] for particle-filled semicrystalline polymers and later observed by others [28, 29, 32, 33] for different polypropylene composites.

It should also be noted that the mechanism mentioned above could only be observed around very small particles in the present investigation.

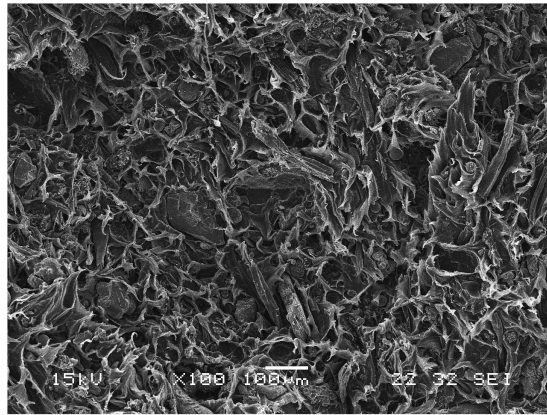
3.5. Fracture Surface Analysis

Figures 7 and 8 show the fracture surfaces of composite SENB samples with raw ash and treated ash, respectively examined by SEM. Matrix ductile tearing is clearly observed in all micrographs, confirming the ductile behavior exhibited by the composites in fracture tests. It is also seen in this figure that there are many ash particles with diameters within the expected range and only a few large particles, as mentioned before.

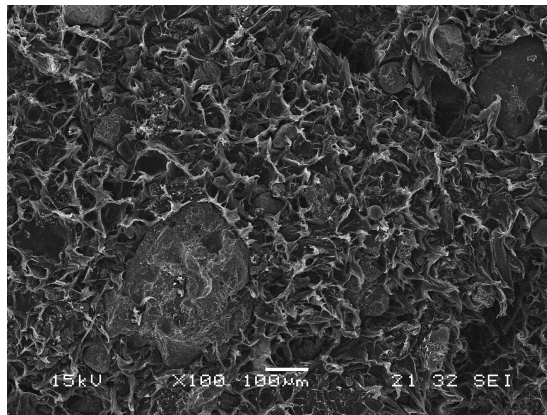
Figure 9(a) and 9(b) shows the energy-dispersive X-ray analysis results obtained from a line that crosses the ash particle and the interface. As can be observed in this figure, the presence of several elements other than carbon such as Al, Si, Ca, etc. (compare Table 2 with Table 3) indicated that the treatment with silane led to the formation of an interface. Hence, filler–matrix interaction seemed to be improved by this treatment.

Silane coupling agents are silicon-based chemicals that contain two types of reactivity (inorganic and organic in the same molecule). A typical general structure is $Y-Si(OR)_3$ where OR is a hydrolyzable group such as methoxy, ethoxy, or acetoxy, and Y is an organofunctional group such as amino, methacryloxy, epoxy, vinyl, etc.

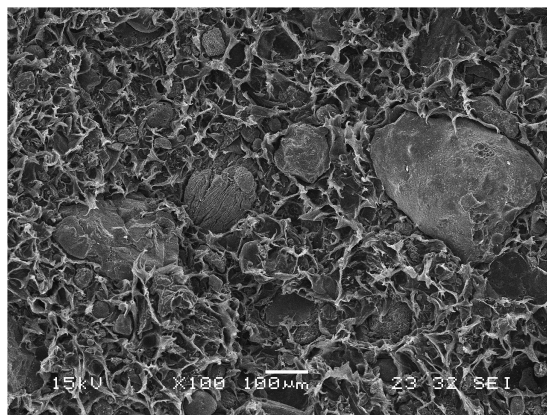
A silane coupling agent will act as a link between an inorganic substrate (such as ash) and an organic material (such as commercial polypropylene) to bond, or couple, the two dissimilar materials together. Although it is usual to pretreat the surfaces of mineral fillers with the silane coupling agent, it may also be added to the



(a)

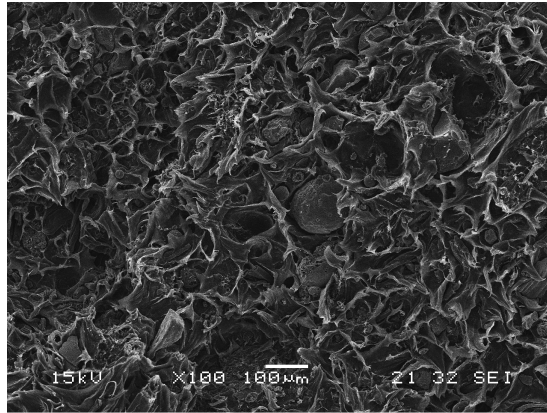


(b)

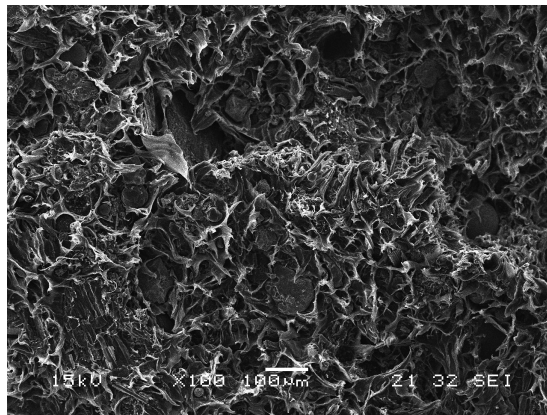


(c)

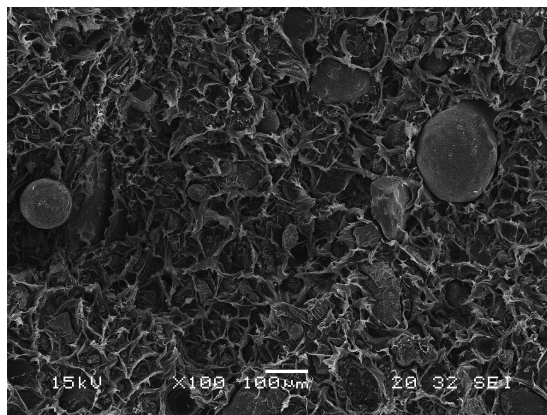
Figure 7. SEM fractographs of the different composite specimens broken in fracture tests: (a) 10 wt% raw ash; (b) 20 wt% raw ash; (c) 30 wt% raw ash.



(a)



(b)



(c)

Figure 8. SEM fractographs of the different composite specimens broken in fracture tests: (a) 10 wt% silane-treated ash; (b) 20 wt% silane-treated ash; (c) 30 wt% silane-treated ash.

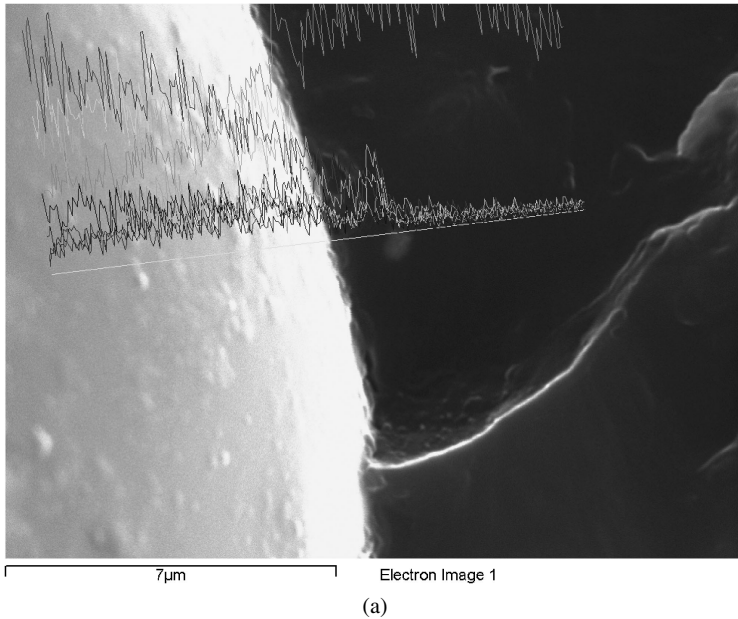


Figure 9. Energy-dispersive X-ray results: (a) Micrograph showing a line that crosses an ash particle and the interface; (b) distribution of the different elements as function of distance.

blend of filler and polymer directly. Polycondensation of the trimethoxy-silyl group also proceeds rapidly: it is already completed in the starting phase of the reaction. The silane coupling agent is selected according to the organic functionality of the target polymer (in this case, an amino group).

The methoxysilyl group is subject to hydrolysis in water or water/alcohol solutions. The initial product of hydrolysis is a silanetriol: $\text{RSi}(\text{OCH}_2\text{CH}_3)_3 + 3\text{H}_2\text{O} \rightarrow \text{RSi}(\text{OH})_3 + 3\text{CH}_3\text{CH}_2\text{OH}$.

Silanetriols are moderately stable at dilute concentrations in polar solvents such as water and alcohols.

Silanol groups are capable of condensing with hydroxyl groups at the surface of ash filler, as shown in Fig. 10. So silanol groups condensed with hydroxyl groups at the surface of ash.

After condensing with the ash surface, the remaining silanol groups are capable of hydrogen bonding or condensing with adjacent silanol groups. By this combination of covalent and hydrogen bonding, the coupling agent is bonded to the inorganic surface, and modifies it so that it is organo-reactive.

The coupling agent containing a primary amine as organofunctional group reacts instantaneously with the carboxyl groups of the polymer forming secondary amide bonds. During processing, the secondary amide groups take part in further reactions with the continuously forming carboxyl groups, resulting in imide groups. These fast reactions of the silane and the polymer might lead to the enhanced interaction between the components of PP/ash composites.

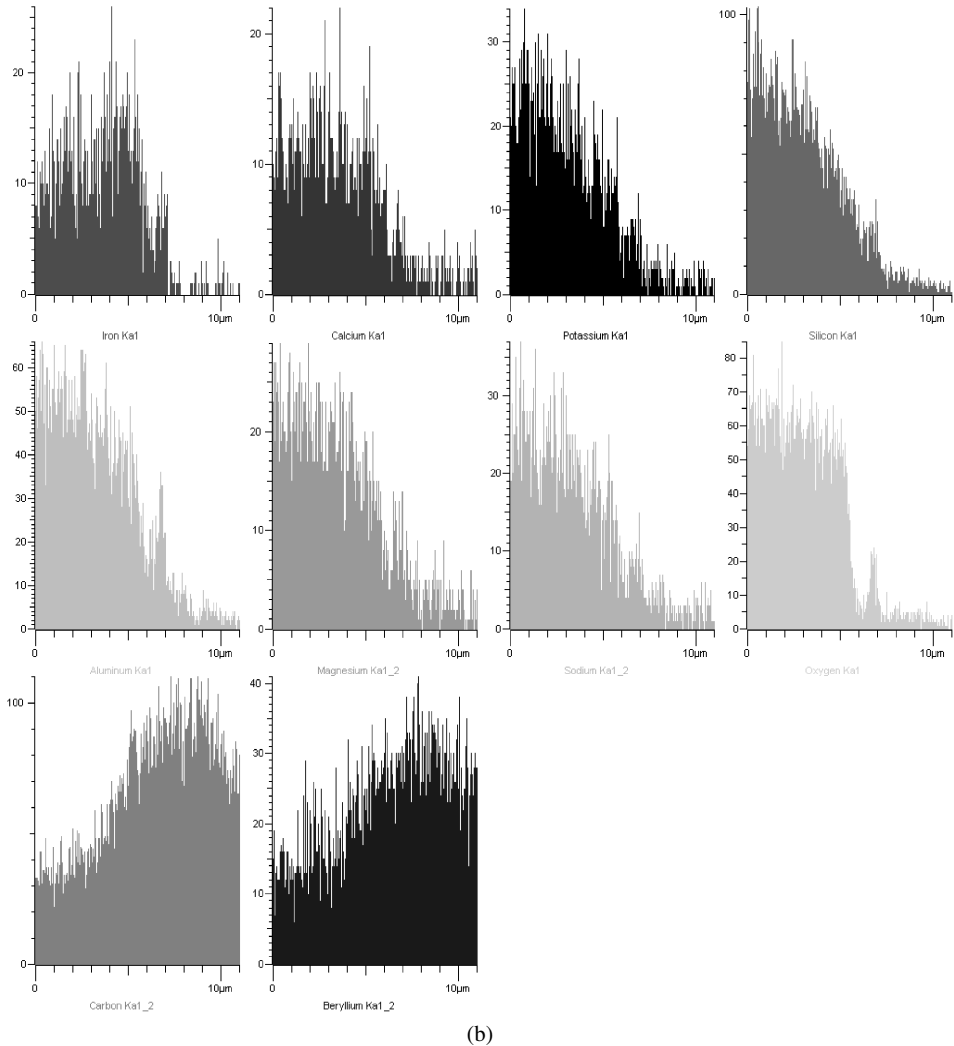


Figure 9. (Continued.)

From the above results, the following conclusions can be drawn.

As a result of poor adhesion, the debonding of small ash particles induced the deformation mechanism in the matrix, which led to higher energy absorption in both the crack initiation and propagation steps. Hence, the composites displayed G_{IQ} and G_{CP} values higher than those of the PP matrix.

On the other hand, debonding of large particles did not seem to contribute to the deformation mechanism but led to the formation of critical-size flaws. Therefore, the increase in ash content led to a decrease in the tensile and fracture properties due to the greater number of large particles able to induce premature failure.

Finally, the incorporation of the silane coupling agent was expected to improve the ash particles dispersion in the matrix and/or increase the interaction between

Table 2.

Chemical composition of ash

Element	Approximate concentration	Intensity cornn.	Weight%	Weight% sigma	Atomic%
C K	36.56	0.4217	35.27	2.57	48.85
O K	38.33	0.4668	33.39	1.57	34.72
Na K	2.73	0.7077	1.57	0.18	1.14
Mg K	1.37	0.6678	0.83	0.11	0.57
Al K	14.76	0.7771	7.72	0.33	4.76
Si K	18.86	0.7722	9.93	0.42	5.88
K K	9.85	1.0183	3.93	0.18	1.67
Ca K	4.02	0.9501	1.72	0.09	0.71
Ti K	0.53	0.8056	0.27	0.05	0.09
Mn K	0.39	0.7970	0.20	0.06	0.06
Fe K	10.32	0.8127	5.17	0.24	1.54
Totals			100.00		

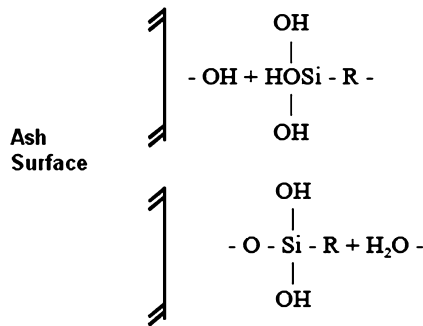
Note: The symbol K represents the K-lines which are emitted by a chemical element and are typical of X-ray diffraction analysis.

Table 3.

Chemical composition of the PP matrix

Element	Approximate concentration	Intensity cornn.	Weight%	Weight% sigma	Atomic%
C K	181.32	2.1635	100.00	0.00	100.00
Totals			100.00		

Note: The symbol K represents the K-lines which are emitted by a chemical element and are typical of X-ray diffraction analysis.

**Figure 10.** Schematic of the silane chemical mechanism.

PP and ash. The latter effect was confirmed by the results obtained from energy-dispersive X-ray analysis.

As has been established in the literature [34], weaker interaction between rigid particles and the polymer matrix leads to higher toughness as the debonding process is favored. Therefore, the slight improvement in the materials fracture properties obtained from the silane treatment should be attributed more to other effects rather than to the increased interaction between PP and ash.

Although no significant evidence of the improvement of the dispersion of ash particles in the matrix as a result of the silane treatment was found, this effect could be considered at least in part, as responsible for the slight increase in the materials' fracture properties observed.

In addition, the presence of ash could also influence the crystallization behavior of PP in different ways. On one hand, the presence of the filler could induce changes in the degree of crystallinity and in the thickness of lamellae as well as some deviation of the lamellar size distribution mostly in the near-interface regions [35]. On the other hand, the particle–matrix interfaces promote a preferential form of crystallization over a definite distance around the particles. The lowest energy surfaces of crystalline lamellae represent also the crystallographic planes of lowest plastic resistance which lie parallel to the interfaces. Thus, crystalline layers of large plastic anisotropy able to affect the material fracture behavior are created [36–38]. Thermal analysis is in progress to elucidate the effect of the silane treatment on the crystallization behavior of PP.

4. Conclusions

The deformation and fracture behavior of PP/ash composites with different ash content was investigated. The effect of a silane coupling agent was also analyzed.

From tensile tests, an increase in the stiffness with ash content was found as a result of the incorporation of such stiffer filler to the PP matrix. In contrast, a decrease in tensile strength and ultimate strain with filler loading was observed. Poor interfacial adhesion between both phases led to large particle debonding from the matrix and the subsequent critical-size flaws formation. The number of debonded large particles increased with filler content.

In addition, the composites displayed higher values of fracture parameters than the matrix as a result of the development of a small particle-induced toughening mechanism. However, fracture properties were also found to decrease with ash content. This could be attributed to the increase in the number of critical-size flaws that induced premature failure.

The incorporation of a silane coupling agent into the formulations led to composites with slightly improved tensile and fracture properties as a result of a better dispersion of ash particles in the matrix, changes in the crystallization behavior of PP and/or improved interaction between PP and ash. The latter effect was confirmed from the results of energy-dispersive X-ray analysis.

References

1. S. Bose and P. A. Mahanwar, Effect of flyash on the mechanical, thermal, dielectric, rheological and morphological properties of filled Nylon-6, *J. Miner. Mater. Charact. Engng* **3**, 65–72 (2004).
2. P. M. Stefani, V. Cyras, A. Tejeira Barchi and A. Vázquez, Mechanical properties and thermal stability of rice husk ash filled epoxy foams, *J. Appl. Polym. Sci.* **99**, 2957–2965 (2006).
3. P. M. Stefani, D. García, J. Lopez and A. Jiménez, Thermogravimetric analysis of composites obtained from sintering of rice husk-scrap tire mixtures, *J. Therm. Anal. Cal.* **81**, 315–320 (2005).
4. D. S. Chaudhary, M. C. Jollands and F. Cser, Recycling rice hull ash: a filler material for polymeric composites?, *Adv. Polym. Tech.* **23**, 147–155 (2004).
5. M. Wang, Z. Shen, C. Cai, S. Ma and Y. Xing, Experimental investigations of polypropylene and poly(vinyl chloride) composites filled with perospheres, *J. Appl. Polym. Sci.* **92**, 126–131 (2004).
6. S. Siriwardena, H. Ismail and U. S. Ishiaku, Effect of mixing sequence in the preparation of white rice husk ash filled polypropylene/ethylene-propylene-diene monomer blend, *Polymer Testing* **20**, 105–113 (2000).
7. S. Siriwardena, H. Ismail and U. S. Ishiaku, A comparison of the mechanical properties and water absorption behavior of white rice husk ash and silica filled polypropylene composites, *J. Reinf. Plast. Compos.* **22**, 1645–1667 (2003).
8. H. Ismail, H. B. Hong, C. Y. Ping and H. P. S. Abdul Khalil, The effects of a compatibilizer on the properties of polypropylene/silica/white rice husk ash hybrid composites, *J. Reinf. Plast. Compos.* **21**, 1685–1712 (2002).
9. R. A. Kruger, M. Hovy and D. Wardle, The use of fly ash filler in rubber, in: *Proc. Intl Ash Utilization Symposium*, Paper 72, Kentucky, USA (1999).
10. J. Y. Hwang, Beneficial Use of Fly Ash, National Energy Technology Department, US Department of Energy, USA, <http://www.netl.doe.gov/>
11. N. Chand and S. R. Vashishtha, Melt flow studies of flyash particulate filled pp/pMMA blend, *Clay Research* **19**, 49–56 (2000).
12. N. Chand, N. Khare and J. Indian, Effect of coupling agents on the mechanical properties of fly ash composites, *Engng Mater. Sci.* **6**, 342 (1999).
13. N. Chand and N. Khare, Effect of flyash loading on dielectric relaxation of polypropylene/low density polyethylene blends, *Met. Mater. Process* **12**, 319–326 (2000).
14. N. Chand and A. Pandey, High stress abrasive wear study on flyash filled polypropylene/polystryrene blends, *Met. Mater. Process* **12**, 91–95 (2000).
15. J. Pionteck, V. B. Sadhu, L. Jakisch, P. Pötschke, L. Häubler and A. Janke, Crosslinkable coupling agents: synthesis and use for modification of interfaces in polymer blends, *Polymer* **46**, 6563–6574 (2005).
16. S. Thongsang and N. Sombatsompop, Effect of NaOH and Si69 treatments on the properties of fly ash/natural rubber composites, *Polym. Compos.* **27**, 30–40 (2005).
17. S. G. Pardo, C. Bernal, M. J. Abad and J. Cano, Composite materials based on polypropylene reinforced with fly ash, *J. Appl. Polym. Sci.* (submitted).
18. Standard test method of tensile properties of plastics; ASTM D638-03, American Society for Testing and Materials, New York, USA (2003).
19. Standard test methods for plane-strain fracture toughness and energy release rate determination of plastics materials; ASTM D5045-93, American Society for Testing and Materials, New York, USA (1993).
20. M. J. Adams, D. Williams and J. G. Williams, The use of linear elastic fracture mechanics for particulate solids, *J. Mater. Sci.* **24**, 1772–1776 (1989).

21. T. Matsunaga, J. K. Kim, S. Hardcastle and P. K. Rohatgi, Crystallinity and selected properties of fly ash particles, *Mat. Sci. Engng* **325**, 333–343 (2002).
22. A. Stocchi, A. Vázquez and C. Bernal, Deformation and fracture behavior of vinyl ester/fly ash composites, *Polym. Compos.* (submitted).
23. S.-C. Won and Y.-W. Mai, Effect of rubber functionality on microstructures and fracture toughness of impact-modified nylon 6,6/polypropylene blends: 1. Structure–property relationships, *Polymer* **40**, 1553–1566 (1999).
24. P. M. Frontini and A. Fave, The effect of annealing temperature on the fracture performance of isotactic polypropylene, *J. Mater. Sci.* **30**, 2446–2454 (1995).
25. E. Santarelli and P. Frontini, The effects of specimen size and testing conditions on fracture toughness evaluation of polypropylene homopolymer, *Polym. Engng. Sci.* **41**, 1803–1814 (2001).
26. J. G. Williams, in: *Fracture Mechanics of Polymers*. Ellis Horwood Limited, London, UK (1984).
27. R. Gensler, C. J. G. Plummer, C. Grein and H. H. Kausch, Influence of the loading rate on the fracture resistance of isotactic polypropylene and impact modified isotactic polypropylene, *Polymer* **41**, 3809–3819 (2000).
28. T. Vu-Khanh and B. Fisa, Effects of fillers on fracture performance of thermoplastics: strain energy density criterion, *Theor. Appl. Fracture Mech.* **13**, 11–19 (1990).
29. T. Vu-Khanh and B. Fisa, Fracture behavior of mica-reinforced polypropylene: effects of coupling agent, flake orientation, and degradation, *Polym. Compos.* **77**, 219–226 (1986).
30. G. M. Kim and G. H. Michler, Micromechanical deformation processes in toughened and particle-filled semicrystalline polymers: Part 1. Characterization of deformation processes in dependence on phase morphology, *Polymer* **39**, 5689–5697 (1998).
31. G. M. Kim and G. H. Michler, Micromechanical deformation processes in toughened and particle-filled semicrystalline polymers. Part 2: Model representation for micromechanical deformation processes, *Polymer* **39**, 5699–5703 (1998).
32. W. C. J. Zuiderdein, C. Westzaan, J. Huétink and R. J. Gaymans, Toughening of polypropylene with calcium carbonate particles, *Polymer* **44**, 261–275 (2003).
33. A. Lazzeri, S. M. Zebarjad, M. Pracella, K. Cavalier and R. Rosa, Filler toughening of plastics. Part 1. The effect of surface interactions on physico-mechanical properties and rheological behaviour of ultrafine CaCO₃/HDPE nanocomposites, *Polymer* **46**, 827–844 (2005).
34. Y. S. Thio, A. S. Argon and R. E. Cohen, Role of interfacial adhesion strength on toughening polypropylene with rigid particles, *Polymer* **45**, 3139–3147 (2004).
35. Z. Bartczak, A. S. Argon, R. E. Cohen and M. Weinberg, Toughness mechanism in semicrystalline polymer blends: II. High-density polyethylene toughened with calcium carbonate filler particles, *Polymer* **40**, 2347–2365 (1999).
36. O. K. Moratoglu, A. S. Argon, R. E. Cohen and M. Weinberg, Toughening mechanism of rubber-modified polyamides, *Polymer* **36**, 921–930 (1995).
37. M. W. L. Wilbrink, A. S. Argon, R. E. Cohen and M. Weinberg, Toughenability of Nylon-6 with CaCO₃ filler particles: new findings and general principles, *Polymer* **42**, 10155–10180 (2001).
38. Y. S. Thio, A. S. Argon, R. E. Cohen and M. Weinberg, Toughening of isotactic polypropylene with CaCO₃ particles, *Polymer* **43**, 3663–3674 (2002).